Research Article | Vol. 28, No. 3 / 3 February 2020 / Optics Express 3779
Optics EXPRESS

Sensitivity analysis of Raman endoscopy with and without wavefront shaping

LYUBOV V. AMITONOVA[1,2,*] AND JOHANNES F. DE BOER[1]

[1]LaserLaB, Department of Physics and Astronomy, Vrije Universiteit Amsterdam, De Boelelaan 1081, 1081 HV Amsterdam, The Netherlands
[2]Advanced Research Center for Nanolithography, Science Park 106, 1098 XG Amsterdam, The Netherlands
[*]l.amitonova@vu.nl

Abstract: Vibrational spectroscopy is a powerful method for the label-free identification of molecules. Spontaneous Raman spectroscopy integrated with an ultra-thin fiber-based endoscope can provide remote, local, and minimally invasive chemical analysis in many fields from biomedical diagnostics to the materials industry. Miniaturization of the probe in combination with a large field of view (FOV) and high sensitivity would be beneficial for a broad class of applications. Here we quantitatively analyze signal-to-noise ratio (SNR) and the sensitivity improvement due to wavefront shaping. We show that wavefront shaping in an ultra-thin single-fiber probe allows to decrease the total measurements time up to several orders of magnitude even without any prior knowledge of the Raman particle location. Such a fiber probe is well suited for minimally-invasive endoscopy in biological and medical applications.

1. Introduction

Inelastic scattering of light offers a broad variety of powerful label-free tools for monitoring processes in the biomedical field and materials industry [1]. Remote-detection at a fiber tip would be beneficial in many applications, such as detection of environmental contaminants [2], diagnosis of cancer [3] or Alzheimer's disease [4]. Over the past years, a variety of fiber probes optimized for Raman interrogation have been demonstrated [5–8]. Small sub-mm Raman probes are especially important for *in vivo* endoscopy [9] or optical biopsy [10]. Miniature fiber probes have shown to be able to provide Raman imaging in endoscopy settings. The use of a 300 μm fiber bundle with a proper detection setup allowed Raman endo-microscopy for the first time [11].

New perspectives have opened up by the emergence of the wavefront shaping technique, a method that allows light to be focussed behind highly scattering materials [12–14]. Wavefront shaping helps to increase the Raman signal from larger depth [15], to improve contrast of coherent anti-Stokes Raman scattering (CARS) microscopy [16], and to enhance the intensity of Raman high-order sidebands [17]. Adaptive wavefront shaping technique allows control and optimization of the stimulated Raman scattering (SRS) in multimode fibers [18]. With the help of wavefront shaping, a conventional step-index multimode (MM) fiber can be utilized as an ultra-thin aberration-free imaging probe [19–21]. MM fibers have become a very promising tool for endo-microscopy applications [22–24]. A single step-index MM fiber with a diameter of 125 μm was demonstrated as the smallest footprint Raman imaging fiber probe [25]. Recently, Raman chemical imaging within optically cleared samples through a MM fiber was shown [26].

The sensitivity of fiber-based Raman detection still is a big issue due to an additional Raman and fluorescent background from the fiber probe itself. Separate fibers for excitation and detection can be used to overcome this problem and provide a relatively low acquisition time of 1–60 s [5–10]. However, it significantly increases the probe diameter and simultaneously limits the field of view (FOV), decreasing the probability to detect rare small particles. Hollow-core fibers have shown to enable highly sensitive detection by reducing the level of the background compared to standard index-guiding optical fibers [27,28]. However, such fibers are expensive and work

#383801 https://doi.org/10.1364/OE.383801
Journal © 2020 Received 25 Nov 2019; revised 10 Jan 2020; accepted 13 Jan 2020; published 27 Jan 2020

Optics EXPRESS

only within a limited wavelength range. Recently, a sapphire optical fiber, with its inherent low background due to its crystalline nature were proposed for Raman imaging in a broad frequency range [29]. However, this fiber has no cladding and needs an air surrounding, which limits its use for endoscopic applications. Moreover, the crystalline nature makes the sapphire fiber not so flexible. Consequently, the search for optimal miniature fiber probes and new experimental procedures for high-sensitive Raman detection is still ongoing.

Here we address the question of sensitivity of Raman endoscopy with and without wavefront shaping. We use the approach proposed by Gusachenko et al. [25] and show that wavefront shaping is beneficial not only for imaging purposes but also for the SNR enhancement of Raman endoscopy. We demonstrate a method that significantly improves the sensitivity of Raman measurements through a miniature single-fiber probe by more than an order of magnitude, which opens new avenues toward minimally invasive Raman endoscopy. We carefully analyze the signal-to-noise ratio (SNR) for conventional and wavefront shaping based approaches of Raman endoscopy. Our theoretical analysis shows that wavefront shaping increases the sensitivity of Raman endoscopy through an ultrathin Raman probe by more than three orders of magnitude for an arbitrarily positioned Raman active particle anywhere in the FOV. This means that the detection time can be decreased without sacrificing the SNR. We carefully analyze the limits of the proposed approach and experimentally demonstrate a sensitivity enhancement by a factor of 20.

2. Experimental setup and optimization procedure

Our experiments were performed on a conventional step-index MM fiber (Thorlabs, FG105UGA) with a silica core of 105 μm diameter, a numerical aperture NA = 0.2 and a length of approximately 15 cm. This fiber provides a ratio of the FOV diameter (105 μm) and the total diameter (125 μm) close to 1. The pump beam was provided by the second-harmonic output of a continuous-wave Nd:YAG laser with a wavelength of 532 nm [Cobolt Samba]. The experimental setup is presented in Fig. 1. The laser beam was expanded by a lens-based telescope 6.67 times in order to match the surface of our spatial light modulator. For that, we used a telescope consisted of two lenses 1 inch in diameter and focal lengths of 30 mm and 200 mm.

We used a Vialux V4100 digital micromirror device (DMD) with a resolution of 1920×1200 pixels and a pixel size of 10.8 μm. To control it, we used the custom made software written in Labview and based on ALP-4.1 high-speed application programming interface (alpD41.dll) provided by Vialux. We chose to use a DMD as a spatial light modulator (SLM) for several reasons. Primarily, due to its modulation speed that exceed by several orders of magnitude the refresh rate of well-known liquid crystal SLMs. It allowed us to significantly decrease optimization time, which was finally limited by the speed of the detector. With a high-speed camera [Basler] running at 320 frames/sec, the wavefront shaping procedure required no more than 6 seconds. Switching between optimized wavefronts can be done at the speed of the DMD (10 kHz). Moreover, the DMD can achieve better beam-shaping fidelity compared to liquid-crystal SLMs, as was shown by Turtaev et al. [30]. One reason for this better performance is that DMDs suffer less from scattering, which is present in liquid crystal SLMs and contributes to an uncontrolled background distorting the wavefront shaping procedure.

For wavefront shaping, we implemented a 'stepwise sequential algorithm' [31]. We exploited the DMD for spatial phase modulation (phase only control) by the Lee holography method [32]. Each mirror of the DMD can be set to two different tilt angles. The mirrors were used to create a binary 2D grating with a period of 10 micromirrors. The DMD area illuminated by the beam was divided into 625 segments: square groups of 25×25 micromirrors. Lenses placed in a 4f-configuration were used to image the phase mask on the back focal plane of a coupling objective (10x, NA = 0.25). A pinhole in the Fourier plane blocked all the diffraction orders except the 1st, encoding the desired spatial phase distribution. We individually modulated

Optics EXPRESS

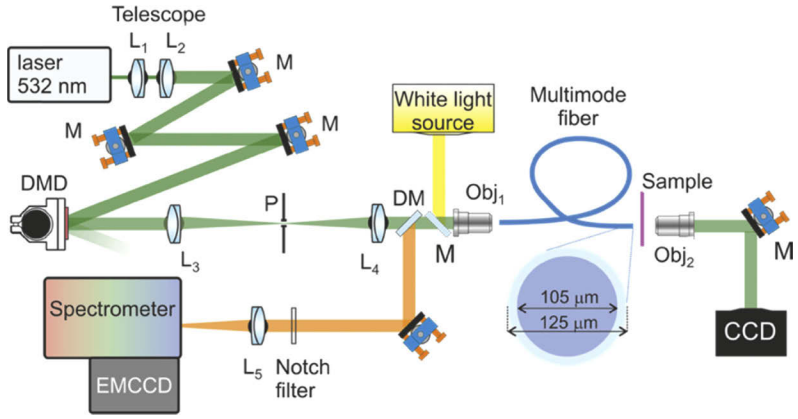

Fig. 1. Sketch of the experimental setup. The pre-calibration part of the setup is only used at the beginning of each experiment for wavefront optimization. Raman detection and imaging are done in an endoscopy configuration (backward direction). The MM fiber with a FOV diameter of 105 µm and total probe diameter 125 µm was used to deliver the pump light to a sample, collect the Raman response and propagate it to the detection system. Bright-field microscopy was used to get a reference image of the sample. DMD, digital micromirror device; M, mirror; DM, dichroic mirror; P, pinhole; EMCCD, Electron Multiplying Charge-Coupled Device; L, plano-convex lenses (L_1, $d_1 = 1$", $f_1 = 30$ mm; L_2, $d_2 = 1$", $f_2 = 200$ mm; L_3, $d_3 = 2$", $f_3 = 150$ mm; L_4, $d_4 = 1$", $f_4 = 100$ mm; L_5, $d_5 = 1$", $f_5 = 100$ mm); Obj, Olympus Plan Achromat Objectives (Obj_1, 10x, NA = 0.25; Obj_2: 20x, NA = 0.4).

the phase of each segment by spatially shifting the corresponding grating pattern between 0 and 2π in three steps of $2\pi/3$ each. All the other segments were kept static and served as a co-propagating reference beam. The second microscope objective (20x, NA = 0.4) was used to image the distal end of the fiber on the CCD camera (Basler). At the camera, the light from the modulated segment interferes with the light originated from reference segments. In total 1875 frames were measured for a single wavefront shaping procedure. For each modulated segment, the phase leading to the highest intensities in each spot on the fiber output was calculated by fitting a cosine function over three measurement points. By repeating the measurement for each DMD segment, the optimal phase pattern was reconstructed and the intensity on each target spot can be enhanced relative to the uncontrolled initial speckle pattern. The wavefront shaping procedure was done once before the measurements and can be done with any 2D spatial light modulator. Laser power on the fiber output was 1.5 mW.

To characterize the fidelity of wavefront shaping, we define the parameter $\gamma^2 = P_{focus}/P_0$, where P_{focus} is the power integrated over the dimensions of the focused spot and P_0 is the total power transmitted through the fiber. The average wavefront shaping fidelity of our setup was measured to be $\gamma^2 = 0.2$ leading to the maximum power density about 10^4 W/cm^2.

Raman detection and imaging were done in the backward direction suitable for endoscopy. The same MM fiber was used to collect the total Raman signal from the sample and propagate it back to the detection system. We used a dichroic mirror to separate the signal from the excitation light and an additional Notch filter to remove the last remaining excitation light. A spectrometer (Shamrock Andor) with a grating pitch of 1200 *l*/mm and a slit width of 200 µm and a high sensitive electron-multiplying CCD (EMCCD) camera (iXon Andor) were used for the detection. The size of the input slit was chosen as a compromise between the resolution and light collection efficiency from the large core fiber probe. The resulting spectral resolution was 50 cm^{-1}, which is twice bigger than in [25]. Nevertheless, it allowed us to detect the broad Raman band of C-H

Optics EXPRESS

vibrations of polystyrene by using both approaches with and without wavefront shaping. The spectral resolution can be further improved by optimizing parameters of the spectrometer.

3. Theoretical analysis

Firstly, we theoretically analyze the best possible sensitivity of conventional Raman endoscopy through a single fiber and the sensitivity improvement of Raman endoscopy by wavefront shaping. The main goal is to present a Signal to Noise analysis for the detection of an arbitrarily positioned small Raman active particle with an ultrathin fiber probe in the presence of background noise. We use a standard step-index MM fiber with a core radius R. We assume that the radius of a Raman particle, r, is significantly smaller than the fiber core radius, $r << R$. To realize a large FOV, we use a large core MM fiber, resulting in a speckled illumination pattern on the fiber output facet. Due to the speckle pattern, the laser power illuminating the Raman active particle (P_s) depends on its position, but on average P_s is proportional to the ratio of the Raman particle area ($S_r = \pi r^2$) and the fiber facet area ($S_R = \pi R^2$), $P_s = P_0\, S_r/S_R$, where P_0 is the total laser power propagating through the fiber. We assume that the total power is low enough to avoid causing damaging or photobleaching effects, meaning that the background intensity is constant. More importantly, we assume that the large background, typical for spontaneous Raman detection, is constant during the measurements *and* proportional to the total laser power. The origin of the background is the fluorescence of the sample and fluorescent and/or Raman signals generated in the fiber probe itself. As a fundamental noise level we consider the shot noise of the large background to be the dominant contribution, which is proportional to the square root of the total power. Therefore, the best possible SNR for conventional Raman endoscopy is:

$$SNR_0 \propto \frac{P_s}{\sqrt{P_0}} = \frac{r^2}{R^2}\sqrt{P_0}, \tag{1}$$

where r is the radius of a single Raman particle on the fiber output facet, which we want to detect and R is the fiber core radius. In this case the SNR depends on the size of the Raman active area.

Wavefront shaping allows us to localize the laser light at the desired position on the fiber output facet, significantly increasing the Raman response and, consequently, the SNR. Firstly, we assume that we know the location of a Raman microparticle. Later we will consider a more practical case of an unknown position of the particle. The laser power on the particle after wavefront shaping is proportional to the fidelity γ^2, which quantifies the ability to focus all the light to a particular point on the fiber output facet: $P_s = \gamma^2 P_0$. The large background doesn't change by the wavefront shaping procedure in the case of an uniform background from a sample or a background dominated by signal from the fiber probe. As a result, the SNR for Raman endoscopy through a MM fiber with wavefront shaping can be calculated as:

$$SNR_{wfs} \propto \gamma^2\sqrt{P_0}. \tag{2}$$

We define the total enhancement of the SNR of Raman endoscopy that can be reached by using wavefront shaping as the ratio of SNR_{wfs} and SNR_0:

$$SNR_{gain} = \left(\frac{\gamma R}{r}\right)^2. \tag{3}$$

We assume that the radius of a Raman particle, r, is not smaller than the diffraction limit of a MM fiber probe $r \geq r_{dl}$, where $r_{dl} = \lambda/(4NA)$, λ is the pump wavelength and NA is the fiber numerical aperture. We were working in aberration-free regime, meaning that the size of the focal spot is diffraction-limited and doesn't depend on the radial position [21]. As a result, the SNR for the wavefront shaping case doesn't depend on the Raman active volume anymore. The theoretically

Optics EXPRESS

predicted SNR gain in Raman endoscopy as a function of the normalized radius of a Raman particle $r_{norm} = r/r_{dl}$ is presented in Fig. 2(a). The red curve represents the theoretical maximum of the SNR enhancement for phase-only wavefront shaping, $\gamma^2 = \pi/4$ [12]. The experimentally realizable SNR gain for phase-only wavefront shaping is marked with the red hatched area. The blue curve in Fig. 2(a) represents the theoretically predicted enhancements for our experimental wavefront shaping fidelity, $\gamma^2 = 0.2$. We see that the smaller the particle we need to detect, the greater the SNR gain we can expect due to wavefront shaping. Wavefront shaping can increase the SNR of Raman detection through a miniature probe by more than three orders of magnitude. This means that the detection time can be significantly decreased without deterioration of the SNR.

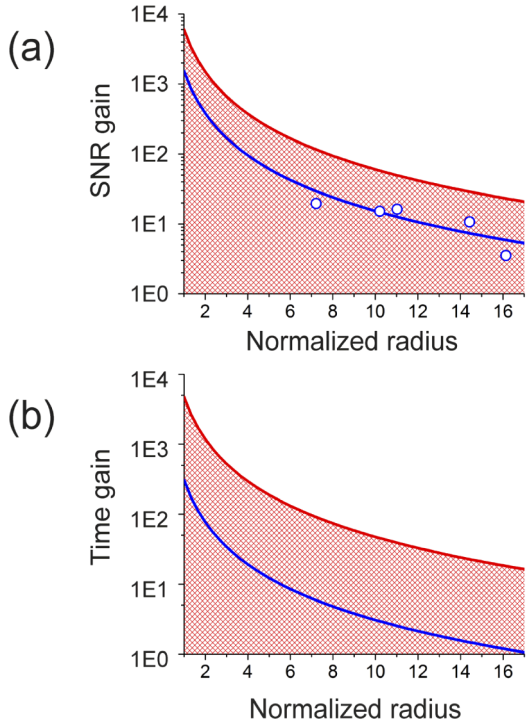

Fig. 2. Sensitivity improvements of Raman detection through a single ultrathin fiber probe with the FOV diameter 105 μm due to the wavefront shaping approach. (a) The SNR gain as a function of the normalized radius of a particle $r_{norm} = r/r_{dl}$, in the case of known location of a Raman particle, where r is the radius of a particle and r_{dl} is a diffraction limit of the MM fiber. (b) The time gain of Raman detection as a function of the normalized radius of a particle, r_{norm}, in the case of an unknown location of the Raman particle. The red and blue curves represent the theoretically predicted data for $\gamma^2 = \pi/4$ and $\gamma^2 = 0.2$, respectively. Open circles show the experimental results for $\gamma^2 = 0.2$.

To determine the ratio of the acquisition times of standard (T_0) and wavefront shaping based (T_{wfs}) Raman endoscopies leading to the same SNR we take into account that the total deposited energy of the incident beam is proportional to the acquisition time:

$$\gamma^2\sqrt{T_{wfs}} = \frac{r^2}{R^2}\sqrt{T_o}. \tag{4}$$

So far, we calculated the SNR gain for a known position of the Raman particle. Now we consider the detection of the particle without knowledge of its location. To analyze the sensitivity and the

Optics EXPRESS

possible time gain we need to take into account the time used for searching for a particle. The maximum number of scanning steps N to cover the full FOV is estimated as the ratio of the FOV and the Raman particle size: $N = (R/r)^2$.

Then we can estimate the time gain, T_{gain}, of Raman detection through an ultrathin fiber probe with a large FOV for an unknown particle position as:

$$T_{gain} = \frac{T_0}{T_{wfs}N} = \left(\frac{\gamma^2 R}{r}\right)^2. \tag{5}$$

The theoretically predicted time gain in Raman endoscopy as a function of normalized radius of a Raman particle $r_{\text{norm}} = r/r_{\text{dl}}$ is presented in Fig. 2(b). The red and blue curves show the time gain for wavefront shaping with fidelity $\pi/4$ and 0.2, respectively.

Figure 2(b) shows that even if the precise location of a small Raman particle is unknown the wave front shaping technique can significantly (by several orders of magnitude) decrease the time needed for the Raman detection through a miniature probe with a large FOV maintaining the same SNR and sensitivity. This is especially important in the case of spontaneous Raman interrogation, which is known to be weak in comparison with the typical fluorescence background.

4. Experimental demonstration of the SNR gain

In the first set of measurements, we analyzed the SNR of standard Raman endoscopy, performed through a thin fiber probe. Six polystyrene microparticles were placed within the fiber FOV, as depicted in Fig. 3. We measured the Raman spectra in background corrected mode (the background was subtracted) with 900 s acquisition time. As background, we used the spectrum measured through the same fiber probe from a clean cover glass substrate. We normalized the spectrum by subtracting the mean value and dividing by the standard deviation value, both measured within the silent region of 3110–3200 cm^{-1}. As a result, the normalized intensity represents also the local SNR. The SNR was estimated as 1.1 by calculating the mean value over a range of 14 cm^{-1} around the Raman peak of the normalized spectrum. For the analysis, we used only the raw data without applying any denoising methods. To present the data more clearly we used an additional smoothing procedure by applying a Savitzky-Golay finite impulse response filter of the first polynomial order and with a length of 7, meaning averaging within a window of 3.5 cm^{-1}, which is less than our actual spectral resolution. The results are presented in Fig. 3 by the blue curve. Despite the relatively large noise, we clearly see a Raman line of polystyrene at approximately 3060 cm^{-1}. We repeated this experiment by varying the number of polystyrene spheres on the fiber output facet from 3 to 15. For a lower number of particles even 20 minutes of acquisition time was not enough to get a Raman signal.

As a sample, we used polystyrene microparticles (Kisker Biotech GmbH) with a mean diameter of 5 μm. We randomly distributed microparticles over a standard glass coverslip by placing a drop of water with dispersed microparticles on the coverslip and letting it dry out. The sample was mounted on a 3D translation stage to allow the interrogation of different microparticle distributions. Bright-field microscopy was used to get a reference image of the sample.

In the second set of measurements, we analyzed how wavefront shaping can increase the SNR of Raman endoscopy. The wavefront on the fiber output facet was optimized to create a focus at the Raman particle (as depicted in Fig. 3). Detection was done in the background corrected mode for different acquisition times from 3 to 30 s. We used the same normalization procedure as described earlier. The SNR for 3 s acquisition time was estimated to be 0.9. The results are presented in Fig. 3 by the red curve and green open circles for 3 and 30 s acquisition times, respectively. To present the data we again used a smoothing procedure by applying a Savitzky-Golay filter.

Figure 3 demonstrates that for a relatively large sample consisting of six spheres each 5 μm in diameter, the SNR of standard Raman endoscopy with an acquisition time of 900 s is

Optics EXPRESS

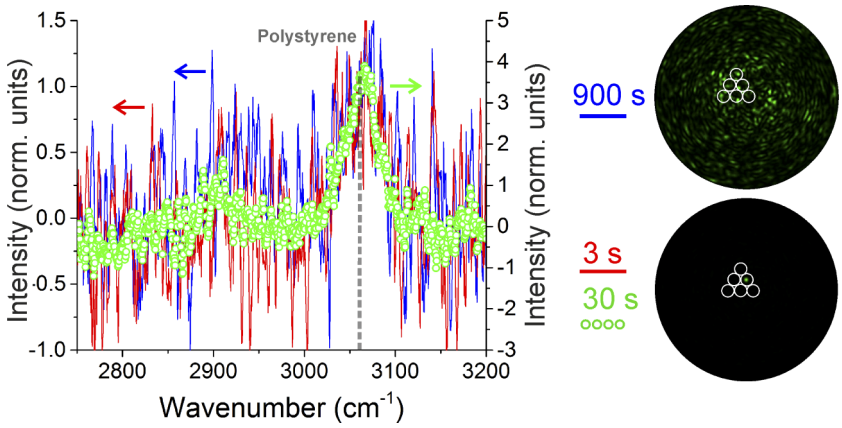

Fig. 3. Normalized Raman spectra measured through an ultra-thin fiber probe by the standard procedure (blue line) and with the help of wavefront shaping (red line and green open circles). Spectra were normalized by dividing by the standard deviation value, measured within the silent region 3110–3200 cm^{-1}. To present the data more clearly we used a smoothing procedure by applying a Savitzky-Golay finite impulse response filter of the first polynomial order and with a length of 7. Acquisition times are 900 s (blue line), 3 s (red line) and 30 s (green open circles). The illustration of the output fiber facets with the Raman particles are presented on the right side for the standard procedure (top) and the proposed approach (bottom).

approximately the same as the SNR of the Raman endoscopy approach improved by wavefront shaping with an acquisition time more than 2 orders of magnitude shorter (only 3 s). As a result, our final acquisition time is relatively low and comparable with other fiber-based Raman endoscopes [5–10] but we a miniature single-fiber probe (the same for excitation and collection) and an order of magnitude lower pump power.

The experimentally measured SNR gain due to wavefront shaping as a function of the effective particle radius is presented in Fig. 2(a) by open circles. In the experiments, we used a different number of Raman particles and estimated the SNR gain as a function of effective radius, which was calculated as $r_{\text{eff}} = r\sqrt{n}$, where n is the total number of particles in the FOV. We see that the experimental data nicely coincides with the theoretically predicted curve. Mismatches can be explained by the randomness of the speckle illumination, especially in the case of a small particle radius.

Our experiments demonstrate the SNR gain for relatively large particle sizes, whereas the maximum SNR enhancement corresponds to small particles. The main reason is that a conventional approach does not allow to detect the signal from a single 5 μm diameter particle even with more than 20 min acquisition time due to high background from our 20 cm fiber probe. At the same time, with wavefront shaping the signal from this single particle was clearly seen with several second acquisition time. As a result, the SNR enchantment is clearly present in case of small particles, however, could not be properly characterized.

5. High-resolution imaging through an ultrathin probe

In the final set of measurements, we demonstrate high-resolution Raman imaging through an ultra-thin fiber probe. We use a fiber that has the same NA but twice larger core diameter than in previous work [25]. This results in a FOV that is twice as large for equal distance from the fiber output facet. The FOV increases with the distance from the fiber output facet (see Ref. [33]) and

Optics EXPRESS

a scale factor determined by the core radius. We experimentally visualize twice smaller objects than in previous Raman endo-microscopy studies [25,26,29].

The Raman images were obtained by raster scanning the focal spot created after the pre-calibration procedure over the FOV with a step size of 0.9 μm. The scanning was performed by changing the DMD phase profile corresponding to different focus positions. For each point, the full Raman spectrum was recorded with an acquisition time of 30 s. The mean value within a bandwidth of 14 cm^{-1} around the expected polystyrene Raman line at 3060 cm^{-1} was used to reconstruct the Raman image.

The results of Raman imaging through a single fiber are presented in Fig. 4. Figure 4(a) shows the bright field image of polystyrene spheres on the fiber output facet, which was used as a reference image. Figure 4(b) represents the Raman image recorded in the backward direction through an ultra-thin endoscope using the procedure described above.

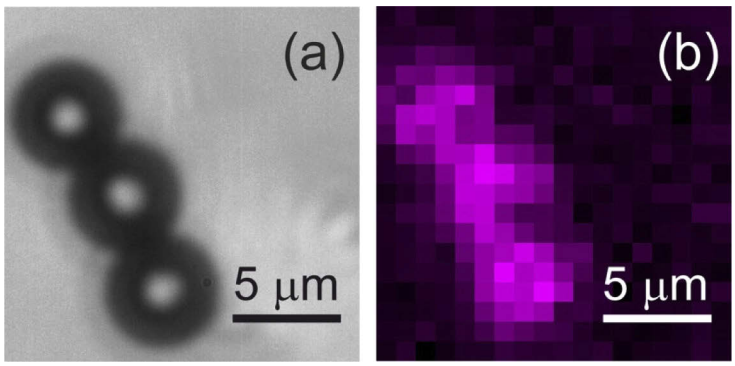

Fig. 4. (a) Bright field image of polystyrene spheres on the fiber output facet used as a reference. (b) Raman image recorded through an ultra-thin fiber endoscope. The diameter of polystyrene spheres is about 5 μm. Laser power on the fiber output is 1.5 mW. The maximum power density is about 10^4 W/cm^2. Scale bars are 5 μm.

Here we focused our attention on the 2D case because it is more relevant for practical endoscopic applications. However, potentially the same approach can be utilized to improve sensitivity in case of 3D imaging through a fiber probe. It is well known that wavefront shaping can create a focused field at some depth in turbid media. In a similar way, focusing at different distances behind the fiber output facet is possible. However, the effective numerical aperture will degrade at larger depths [33].

6. Conclusions

To summarize, we have demonstrated that wavefront shaping is highly beneficial not only for Raman imaging through a thin fiber probe but also allows to significantly increase the sensitivity of Raman endoscopy through a miniature single-fiber probe. Wavefront shaping allows to increase the SNR and, consequently, the sensitivity of fiber-based Raman detection through an ultra-thin probe by three orders of magnitude. As a result, it allows to decrease the total measurements time up to several orders of magnitude even without any prior knowledge of the particle location. Such a fiber probe is well suited for endoscopy in biological and medical applications.

Funding

Stichting voor de Technische Wetenschappen (VENI 15872).

Optics EXPRESS

Acknowledgments

We thank Freek Ariese for fruitful discussions.

Disclosures

The authors declare no conflicts of interest.

References

1. S. Stewart, R. J. Priore, M. P. Nelson, and P. J. Treado, "Raman Imaging," Annu. Rev. Anal. Chem. **5**, 337–360 (2012).
2. L. Zada, H. A. Leslie, A. D. Vethaak, G. H. Tinnevelt, J. J. Jansen, J. F. de Boer, and F. Ariese, "Fast microplastics identification with stimulated Raman scattering microscopy," J. Raman Spectrosc. **49**, 1136–1144 (2018).
3. C. Kendall, M. Isabelle, F. Bazant-Hegemark, J. Hutchings, L. Orr, J. Babrah, R. Baker, and N. Stone, "Vibrational spectroscopy: a clinical tool for cancer diagnostics," Analyst **134**, 1029–1045 (2009).
4. R. Michael, A. Lenferink, G. F. J. M. Vrensen, E. Gelpi, R. I. Barraquer, and C. Otto, "Hyperspectral Raman imaging of neuritic plaques and neurofibrillary tangles in brain tissue from Alzheimer's disease patients," Sci. Rep. **7**, 15603 (2017).
5. T. Yamanaka, H. Nakagawa, M. Ochida, S. Tsubouchi, Y. Domi, T. Doi, T. Abe, and Z. Ogumi, "Ultrafine Fiber Raman Probe with High Spatial Resolution and Fluorescence Noise Reduction," J. Phys. Chem. C **120**, 2585–2591 (2016).
6. I. E. Iping Petterson, J. C. C. Day, L. M. Fullwood, B. Gardner, and N. Stone, "Characterisation of a fibre optic Raman probe within a hypodermic needle," Anal. Bioanal. Chem. **407**, 8311–8320 (2015).
7. J. T. Motz, M. Hunter, L. H. Galindo, J. A. Gardecki, J. R. Kramer, R. R. Dasari, and M. S. Feld, "Optical fiber probe for biomedical Raman spectroscopy," Appl. Opt. **43**, 542–554 (2004).
8. A. S. Haka, Z. Volynskaya, J. A. Gardecki, J. Nazemi, J. Lyons, D. Hicks, M. Fitzmaurice, R. R. Dasari, J. P. Crowe, and M. S. Feld, "In vivo Margin Assessment during Partial Mastectomy Breast Surgery Using Raman Spectroscopy," Cancer Res. **66**, 3317–3322 (2006).
9. Y. Hattori, Y. Komachi, T. Asakura, T. Shimosegawa, G.-I. Kanai, H. Tashiro, and H. Sato, "*In Vivo* Raman Study of the Living Rat Esophagus and Stomach Using a Micro-Raman Probe Under an Endoscope," Appl. Spectrosc. **61**, 579–584 (2007).
10. J. C. C. Day and N. Stone, "A Subcutaneous Raman Needle Probe," Appl. Spectrosc. **67**, 349–354 (2013).
11. L. V. Doronina-Amitonova, I. V. Fedotov, A. B. Fedotov, and A. M. Zheltikov, "High-resolution wide-field Raman imaging through a fiber bundle," Appl. Phys. Lett. **102**, 161113 (2013).
12. I. M. Vellekoop and A. P. Mosk, "Focusing coherent light through opaque strongly scattering media," Opt. Lett. **32**, 2309–2311 (2007).
13. I. M. Vellekoop, A. Lagendijk, and A. P. Mosk, "Exploiting disorder for perfect focusing," Nat. Photonics **4**, 320–322 (2010).
14. J. Jang, J. Lim, H. Yu, H. Choi, J. Ha, J.-H. Park, W.-Y. Oh, W. Jang, S. Lee, and Y. Park, "Complex wavefront shaping for optimal depth-selective focusing in optical coherence tomography," Opt. Express **21**, 2890–2902 (2013).
15. A. M. Paniagua-Diaz, A. Ghita, T. Vettenburg, N. Stone, and J. Bertolotti, "Enhanced deep detection of Raman scattered light by wavefront shaping," Opt. Express **26**, 33565–33574 (2018).
16. A. J. Wright, S. P. Poland, J. M. Girkin, C. W. Freudiger, C. L. Evans, and X. S. Xie, "Adaptive optics for enhanced signal in CARS microscopy," Opt. Express **15**, 18209–18219 (2007).
17. M. Shutova, A. D. Shutov, A. A. Zhdanova, J. V. Thompson, and A. V. Sokolov, "Coherent Raman Generation Controlled by Wavefront Shaping," Sci. Rep. **9**, 1565 (2019).
18. O. Tzang, A. M. Caravaca-Aguirre, K. Wagner, and R. Piestun, "Adaptive wavefront shaping for controlling nonlinear multimode interactions in optical fibres," Nat. Photonics **12**, 368–374 (2018).
19. T. Čižmár and K. Dholakia, "Shaping the light transmission through a multimode optical fibre: complex transformation analysis and applications in biophotonics," Opt. Express **19**, 18871–18884 (2011).
20. R. Di Leonardo and S. Bianchi, "Hologram transmission through multi-mode optical fibers," Opt. Express **19**, 247–254 (2011).
21. A. Descloux, L. V. Amitonova, and P. W. Pinkse, "Aberrations of the point spread function of a multimode fiber due to partial mode excitation," Opt. Express **24**, 18501–18512 (2016).
22. I. T. Leite, S. Turtaev, X. Jiang, M. Šiler, A. Cuschieri, P. S. J. Russell, and T. Čižmár, "Three-dimensional holographic optical manipulation through a high-numerical-aperture soft-glass multimode fibre," Nat. Photonics **12**, 33–39 (2018).
23. S. Ohayon, A. Caravaca-Aguirre, R. Piestun, and J. J. DiCarlo, "Minimally invasive multimode optical fiber microendoscope for deep brain fluorescence imaging," Biomed. Opt. Express **9**, 1492–1509 (2018).
24. D. Loterie, S. A. Goorden, D. Psaltis, and C. Moser, "Confocal microscopy through a multimode fiber using optical correlation," Opt. Lett. **40**, 5754–5757 (2015).
25. I. Gusachenko, M. Chen, and K. Dholakia, "Raman imaging through a single multimode fibre," Opt. Express **25**, 13782–13798 (2017).

Optics EXPRESS

26. I. Gusachenko, J. Nylk, J. A. Tello, and K. Dholakia, "Multimode fibre based imaging for optically cleared samples," Biomed. Opt. Express **8**, 5179–5190 (2017).
27. S. Brustlein, P. Berto, R. Hostein, P. Ferrand, C. Billaudeau, D. Marguet, A. Muir, J. Knight, and H. Rigneault, "Double-clad hollow core photonic crystal fiber for coherent Raman endoscope," Opt. Express **19**, 12562–12568 (2011).
28. L. V. Doronina-Amitonova, I. V. Fedotov, A. B. Fedotov, K. V. Anokhin, M. Hu, C. Wang, and A. M. Zheltikov, "Raman detection of cell proliferation probes with antiresonance-guiding hollow fibers," Opt. Lett. **37**, 4642–4644 (2012).
29. S. Deng, D. Loterie, G. Konstantinou, D. Psaltis, and C. Moser, "Raman imaging through multimode sapphire fiber," Opt. Express **27**, 1090–1098 (2019).
30. S. Turtaev, I. T. Leite, K. J. Mitchell, M. J. Padgett, D. B. Phillips, and T. Čižmár, "Comparison of nematic liquid-crystal and DMD based spatial light modulation in complex photonics," Opt. Express **25**, 29874–29884 (2017).
31. I. M. Vellekoop, "Feedback-based wavefront shaping," Opt. Express **23**, 12189–12206 (2015).
32. W.-H. Lee, "III Computer-Generated Holograms: Techniques and Applications," Prog. Opt. **16**, 119–232 (1978).
33. T. Čižmár and K. Dholakia, "Exploiting multimode waveguides for pure fibre-based imaging," Nat. Commun. **3**, 1027 (2012).